Nalidixic Acid and Fe(II)/Cu(II) Coadsorption at Goethite and Akaganéite Surfaces

Wei Cheng, Jiabin Li, Jie Sun, Tao Luo, Rémi Marsac, Jean-François Boily, Khalil Hanna

Nalidixic Acid and Fe(II)/Cu(II) co-adsorption at goethite and akaganéite surfaces

Wei Cheng[a], Jiabin Li[a], Jie Sun[a], Tao Luo[b,c], Rémi Marsac[d], Jean-François Boily[b], Khalil Hanna[c, *]

[a] College of Resources and Environmental Science, South-Central Minzu University, Wuhan 430074, P.R. China

[b] Department of Chemistry, Umeå University, SE-90187 Umeå, Sweden

[c] Université de Rennes, Ecole Nationale Supérieure de Chimie de Rennes, CNRS, ISCR-UMR 6226, F-35000, Rennes, France.

[d] Université de Rennes, CNRS, Géosciences Rennes - UMR 6118, F-35000 Rennes, France

* Corresponding author: khalil.hanna@ensc-rennes.fr (K. Hanna)

ABSTRACT

Interactions between aqueous Fe(II) and solid Fe(III) oxy(hydr)oxide surfaces play determining roles on the fate of organic contaminants in nature. In this study, the adsorption of nalidixic acid (NA), a representative redox-inactive quinolone antibiotic, on synthetic goethite (α-FeOOH) and akaganéite (β-FeOOH) were examined under varying conditions of pH and cation type and concentration, by means of adsorption experiments, attenuated total reflectance-Fourier transform infrared spectroscopy, surface complexation modeling (SCM) and powder X-ray diffraction. Batch adsorption experiments showed that Fe(II) had marginal effects on NA adsorption onto akaganéite but enhanced NA adsorption on goethite. This enhancement is attributed to the formation of goethite-Fe(II)-NA ternary complexes, without the need for heterogeneous Fe(II)-Fe(III) electron transfer at low Fe(II) loadings (2 Fe/nm^2), as confirmed by SCM. However, higher Fe(II) loadings required a goethite-magnetite composite in the SCM to explain Fe(II)-driven recrystallization and its impact on NA binding. The use of a surface ternary complex by SCM was supported further in experiments involving Cu(II), a prevalent environmental metal incapable of transforming Fe(III) oxy(hydr)oxides, which was observed to enhance NA loadings on goethite. However, Cu(II)-NA aqueous complexation and potential $Cu(OH)_2$ precipitates counteracted the formation of ternary surface complexes, leading to decreased NA loadings on akaganéite. These results have direct implications on the fate of organic contaminants, especially those at oxic-anoxic boundaries.

Keywords: Fe(III) oxy(hydr)oxide; Fe(II); Cu(II); quinolones antibiotics; modeling.

Synopsis

This work shows how the fate of antibiotics can be affected in Fe(II)- and Cu(II)- and FeOOH-bearing environments, such as oxic-anoxic interfaces.

41 **Graphical Abstract**

42

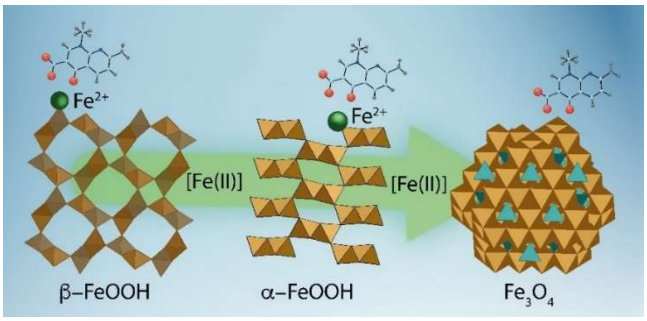

43

44

1. INTRODUCTION

In natural waters and soils, iron can coexist as solid Fe(III) oxy(hydr)oxides minerals and soluble Fe(II), especially at oxide-anoxic boundaries.[1, 2] Electron transfer between sorbed Fe(II) species and solid Fe(III) oxy(hydr)oxide surfaces is an especially important mechanism[3-5] in these settings as it plays a significant role in triggering mineralogical transformations and altering contaminant dynamics in the environment.[6-9] Some Fe(III)-bearing phases can undergo secondary mineralization reactions (ferrihydrite → goethite; lepidocrocite → magnetite)[10-12] following Fe(II) adsorption, while other more stable (goethite,[13] magnetite [4] and hematite[3]) phases can undergo intensive atom exchange without forming new product minerals.

Heterogeneous systems containing Fe(III) oxy(hydr)oxides and Fe(II) are very efficient in environmental remediation due to their high reductive reactivity. Consequently, numerous studies have focused on investigating their efficacy in remediation of both inorganic[6, 14] and organic contaminants.[9, 15, 16] Redox reactions are driven by the high reactivity of adsorbed Fe(II), as the complexation of Fe(II) with Fe(III) oxy(hydr)oxides can significantly lower the redox potential of Fe(II), and thus enhance the reductive reactivity.[9, 17, 18] However, the influence of Fe(II) on the binding capacity of Fe(III) oxy(hydr)oxides has been less studied. The existing research on this subject, limited to a few studies,[7, 8, 19] has chiefly focused on inorganic compounds. For instance, Fe(II) binding onto goethite and hematite was reported to increase adsorption of sulfate and phosphate through ternary complexation and electrostatic interactions.[19] However, Fe(II) had only a minor effect on the fate of arsenate.[7] In contrast, Frierdich et al.[8] found that Fe(II)-induced recrystallization of goethite and hematite

66 repartitioned Ni(II) at the mineral-water interface and substantially altered the fate of Ni(II).
67 Still, little is known about the impact of Fe(II) on the binding of organic, redox-inactive species
68 at Fe(III) oxy(hydr)oxide mineral surfaces. Previous work showed that Fe(II) bound to goethite
69 only slightly enhanced phthalic acid adsorption in the form of ternary outer-sphere species,[9] yet
70 more information on how Fe(II)-organic binding alters Fe(III) oxy(hydr)oxide transformations
71 in these mixed redox systems is needed.

72 This knowledge is especially needed given the increasing scrutiny on the fate of antibiotics
73 (*e.g.* quinolone) in the environment, a consequence of their overuse and incomplete removal by
74 wastewater treatments.[20-22] Our recent studies have showed that Fe(III) oxy(hydr)oxides such
75 as goethite (α-FeOOH), akaganéite (β-FeOOH) and magnetite (Fe_3O_4) play key roles in the
76 mobility and fate of quinolone antibiotics.[23-30] However, Fe(II) coexisting in soils and sediments
77 with Fe(III) oxy(hydr)oxides, resulting from microbial respiration and weathering of Fe-bearing
78 minerals, could also affect the fate of quinolone antibiotics. Two of these minerals were chosen
79 in this study include (i) goethite, which is the most thermodynamically stable iron oxyhydroxide
80 mineral at low-temperature and has significant implications for contaminant mobility in
81 terrestrial and aquatic environments,[31] and (ii) akaganéite, a polymorph of goethite that forms
82 in environments rich in Fe(II) and Cl^-.[32] In addition, OH populations, reactive hydroxyl groups
83 and intrinsic protonation and deprotonation constants were well documented for goethite[23, 25,
84 33, 34] and akaganéite,[35-37] which make them ideal model phases for fundamental interfacial
85 studies.

86 In this work, we investigated the impact of dissolved Fe(II) on the ability of goethite and

akaganéite in binding nalidixic acid (NA), a representative synthetic quinolone antibiotic that is widely present in aquatic and terrestrial environments at concentrations ranging from ng/L to μg/L.[1,38-40] We resolved whether coexisting Fe(II) and NA (i) compete for sorption sites, (ii) cooperatively bind via ternary complexation, and/or (iii) trigger mineralogical transformations. To elucidate these mechanisms, we explored Fe(II) and NA loadings on goethite and akaganéite by batch adsorption and surface complexation modeling, and tracked for phase changes by X-ray diffraction and transmission electron microscopy. We also explored the role of Cu(II), a common trace cation present in groundwater and surface waters alongside Fe(III) oxy(hydr)oxides and antibiotics.[27, 41-43] The inability of Cu(II) to induce transformation of Fe(III) oxy(hydr)oxides provides an opportunity to explore the binding mechanisms in ternary systems (cation/NA/goethite) using attenuated total reflectance-Fourier transform infrared (ATR-FTIR) spectroscopy, without the complication rising from redox-induced mineral transformation and/or possible Fe(II) oxidation. The zeta potential of minerals was also measured to account for the electrostatic effects under various solution chemistry conditions. Our work provides evidence for cation-NA-mineral ternary complexation, and a Fe(II)-concentration/surface loading dependence on the recrystallization of Fe(III) oxy(hydr)oxides.

2. MATERIALS AND METHODS

2.1 Chemicals

Nalidixic acid (NA, $C_{12}H_{12}N_2O_3$), iron(II) chloride tetrahydrate ($FeCl_2 \cdot 4H_2O$), ferric nitrate nonahydrate ($Fe(NO_3)_3 \cdot 9H_2O$), cupric chloride dihydrate ($CuCl_2 \cdot 2H_2O$), hydrochloric acid

(HCl), sodium hydroxide (NaOH), piperazine-1, 4-diethyl sulfonic acid (PIPES) and NaCl were obtained from Sigma-Aldrich. All chemicals used in the study were of pro-analytical quality or better and used as received. Ultrapure "Milli-Q" water (specific resistivity, 18.2 MΩ cm^{-1}) was used for the preparation of all solutions. A stock solution of NA (purity >99%) was prepared by dissolving 232 mg (1 mmole) of NA in 20 mL of 1 M NaOH, followed by dilution to a final volume of 1 L with ultrapure water. All experiments were conducted in an anaerobic chamber (N_2-glovebox, MIKROUNA). All solutions were purged with N_2 for 4 h prior to their introduction into the glovebox.

2.2 Synthesis and characterization of goethite and akaganéite

Goethite[27, 33] and akaganéite[35-37] were synthesized as described in previous studies, and the detailed procedures are given in Text S1(Supporting Information). Phase identity and purity of minerals were confirmed by powder X-ray diffraction (XRD), using a D8 ADVANCE X-ray diffractometer (Bruker, Germany) equipped with a Co X-ray source (λ=0.179 nm). The diffractograms were recorded at 40 kV and 40 mA over 2θ range from 10° to 85° with a 0.02° step size and a collection of 3 s per point. The phases were identified using a MDI Jade 6 software. The size and morphology of as-synthesized minerals were analyzed by transmission electron microscopy (TEM, Tecnai G2 F30 S-TWIN, USA) operated at 300 kV and in bright-field imaging mode. The TEM images indicated that goethite has a typical needle-like shape, with length between 110-150 nm and width of 8-12 nm, while akaganéite presents acicular particles of 4.5-5.7 nm in width and 25-31 nm in length (Figure S1). N_2(g)

adsorption/desorption isotherms were recorded using a nitrogen adsorption apparatus (JWGB SCI.& TECH, JW-BK132F, China) at 77 K before degassing overnight at 353 K, and the calculated B.E.T. specific surface areas were 98 m^2/g for goethite and 183 m^2/g for akaganéite, respectively. The zeta potential of minerals in the presence of different adsorbates was determined using a zeta potential analyzer (NanoBrook 90Plus zeta, Brookhaven, USA). The goethite or akageneite suspensions in the presence of NA and/or cations were adjusted to the desired pH in 10 mM NaCl and equilibrated for 24 h under nitrogen. Aliquots were sampled for ζ determinations and each sample was measured three times with 12 - 30 runs for every measurement. The ζ potential values were averaged over 3 measurements.

2.3 Batch experiments

Adsorption batch experiments were carried out in a glovebox (pO_2 < 1 ppm) to eliminate any O_2-driven redox reactions. Kinetic adsorption studies were conducted in 50 mL polypropylene tubes containing suspensions of 50 m^2/L goethite or akaganéite with 10 μM NA or 300 μM Fe(II) in a background electrolyte of 10 mM NaCl. pH was maintained at 7.0 ±0.1 using PIPES solutions. Aliquots were sampled during the experiments and filtered (0.2 μm, polyethersulfone membrane filter) for analysis. Equilibrium adsorption experiments were conducted in 15 mL polypropylene tubes. Briefly, solutions of 10 or 100 μM NA were mixed with goethite or akaganéite (50 m^2/L) in 10 mM NaCl. $FeCl_2$ (50, 100, 200, 500 μM) or $CuCl_2$ (10, 50, 100 and 200 μM) were added to the solutions in order to study the effects of Fe(II) or Cu(II) on NA adsorption. The pH was then adjusted to the desired value (4 < pH < 10) with 0.1 M HCl or

NaOH solutions. Preliminary experiments showed that adding NA or Fe(II) simultaneously or sequentially after 24 hours of equilibration had negligible effects on adsorption results (Figure S2). Desorption tests were conducted at pH 11 to check the mass balance, and an average recovery of 99 ± 1% confirmed the mass balance. In another set of experiments, adsorption isotherms were collected for varied Fe(II) concentrations (0-500 μM) with 10 μM NA, and the pH was maintained using PIPES solutions at 7.1 ± 0.1. All suspensions were equilibrated on a platform shaker at room temperature for 24 h, and suspension pH values were measured again before filtration (0.2 μm) with a benchtop pH/mV meter (ST3100, Ohaus) calibrated on a daily basis. To investigate the mineral transformations under examination, mixtures of 50 m^2/L goethite or akaganéite in 10 mM NaCl with 10 μM NA and varying concentrations of Fe(II) were prepared at pH 9.0 ± 0.1 for 24 h. The suspensions were then centrifuged and freeze-dried before XRD and TEM characterization.

Aqueous NA concentrations were stored in a refrigerator and determined within 24 h using an Ultimate 3000 high performance liquid chromatography (HPLC) system equipped with a reversed-phase C18 column (250 × 4.6 mm i.d., 5 μm) and a UV detector (258 nm). The mobile phase was a mixture of acetonitrile/water (60:40 v/v) containing 0.1% of formic acid. The flow rate of the mobile phase was set at 1 mL/min in the isocratic mode. Aqueous Fe(II) and Fe(III) concentrations were determined immediately after filtration by the phenanthroline method.[44] Concentrations of Cu(II) were analyzed on an Atomic Absorption Spectrometer (Thermo, ICE-3500). All experiments were performed at least twice, and the reproducibility of the measurements was around 3% for NA and 5% for Fe(II) and Cu(II).

2.4 ATR-FTIR Spectroscopy

Attenuated total reflectance-Fourier transform infrared (ATR-FTIR) spectra of free NA species and bound NA onto goethite with and without Cu(II) were recorded with a Bruker Vertex 70/V FTIR spectrometer equipped with a DLaTGS detector. All spectra were collected in the 600−4000 cm^{-1} range at a resolution of 4.0 cm^{-1} and at a forward/reverse scanning rate of 10 Hz. Each spectrum was an average of 250 scans. The Blackman-Harris 3-term apodization function was used to correct phase resolution. Sample preparation for the ATR-FTIR analysis followed the same procedure as for batch sorption experiments. Two series of experiments were conducted at pH 4-10 in 10 mM NaCl for 50 m^2/L goethite and (i) 100 μM NA or (ii) 100 μM NA with 100 μM Cu(II). Spectra of goethite suspensions in 10 mM NaCl were also taken in the absence of NA and Cu(II) and then subtracted from the spectra of sorbed NA and/or Cu(II) in order to represent surface complexes only. Prior to ATR-FTIR analysis, tubes from batch sorption experiments were centrifuged and then the centrifuged wet pastes were transferred onto a diamond window of an Attenuated Total Reflectance (ATR) cell (Golden Gate, single-bounce). A reference spectrum of aqueous NA was also acquired from a 10 mM NA solution in 1 M NaOH.

2.5 Surface complexation modeling

Surface complexation calculations were performed with PHREEQC (version 2),[45] and using the "minteq.v4" database provided with this geochemical speciation code. The binding behavior at goethite and akaganéite surfaces was described using the multisite complexation (MUSIC) model approach.[46] Detailed information regarding the proportions of crystal planes and

192 corresponding reactive site densities are given in Text S2 in the SI. The electric double layer
193 and electrostatic interactions were described according to the three-plane model (TPM),[46]
194 dividing the mineral–water interface into the 0-, 1-, and 2-planes. Charges of the adsorbates
195 were distributed among the 0 (H^+, metal-bound complex), 1 (hydrogen-bound complex), and 2
196 (Na^+, Cl^-, outer-sphere surface complexes) planes of the TPM and a charge distribution (CD)
197 term was employed for their description only if required. The values of surface site densities
198 and protonation constants, background electrolytes binding constants and capacitances for the
199 0-plane (C1) and 1-plane (C2) were taken from previous studies[23, 24, 27] and are presented in
200 Table S1. The equilibrium constants for the formation of additional surface species are
201 documented in Table 1. The formation constants of NA−Fe(II) and NA−Cu(II) aqueous
202 complex were obtained from the literature.[47] Precipitation of $Fe(OH)_2(s)$ and $Cu(OH)_2(s)$ were
203 taken into account in the calculations (Table S1). Parameters of surface species in simple (binary)
204 systems were individually fitted using independent data sets, and then kept constant for
205 simulations in ternary systems. For example, NA−goethite surface complexation constants were
206 determined using NA adsorption data onto goethite, in close agreement with a previous study,[25]
207 and then kept constant for the rest of simulations. The nature of Fe(II) surface complexes onto
208 goethite has been previously determined[9, 19] and the corresponding surface complexation
209 constants were fitted using the Fe(II) adsorption data obtained in this study. Simulations were
210 then performed in the ternary goethite−Fe(II)−NA system without any parameter adjustment.
211 To mitigate the complexities arising from the precipitation of Cu(II) at high concentrations, we
212 exclusively used the data for Cu(II) at 200 μM for simulation purposes, without employing

213 them for the adjustment of constants. PhreePlot[48], which was used to estimate parameters,
214 employs a parameter optimization procedure that minimizes the weighted sum of squares of the
215 residuals to fit a model to experimental data. A modified Marquardt-Levenberg procedure[49]
216 was applied. With this method, PhreePlot provides also a statistical uncertainty of the estimated
217 parameters (Table 1). For magnetite, we used the 2-pK_a-constant capacitance model approach
218 developed by Jolsterå et al.[50] The reactive site densities were determined as 1.50 sites nm^{-2}, and
219 the capacitance value was estimated as 2.1 F m^{-2}.
220

221 **3. RESULTS AND DISCUSSION**

222 **3.1. Nalidixic Acid adsorption onto goethite and akaganéite**

223 Kinetics experiments showed that NA binding on goethite and akaganéite reached
224 equilibrium within 24 h (Figure S3), and mass balance confirmed that NA was removed only
225 by adsorption.

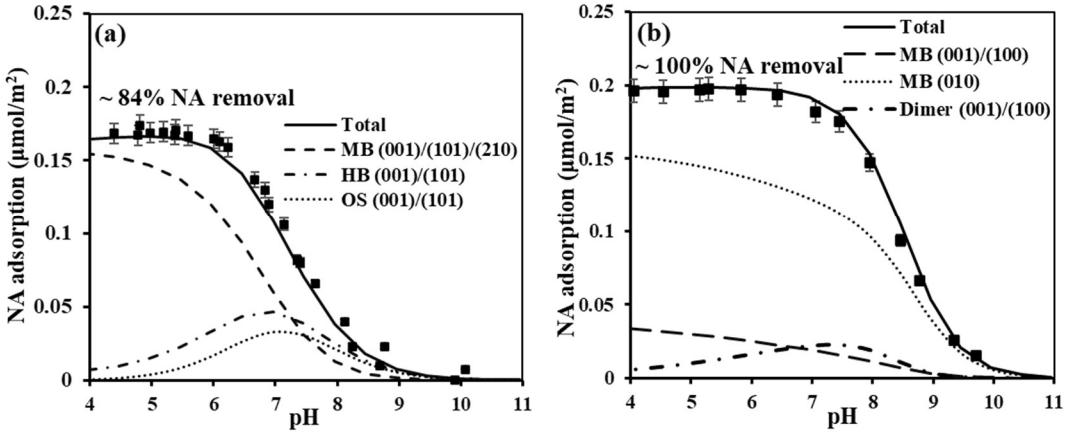

226

227

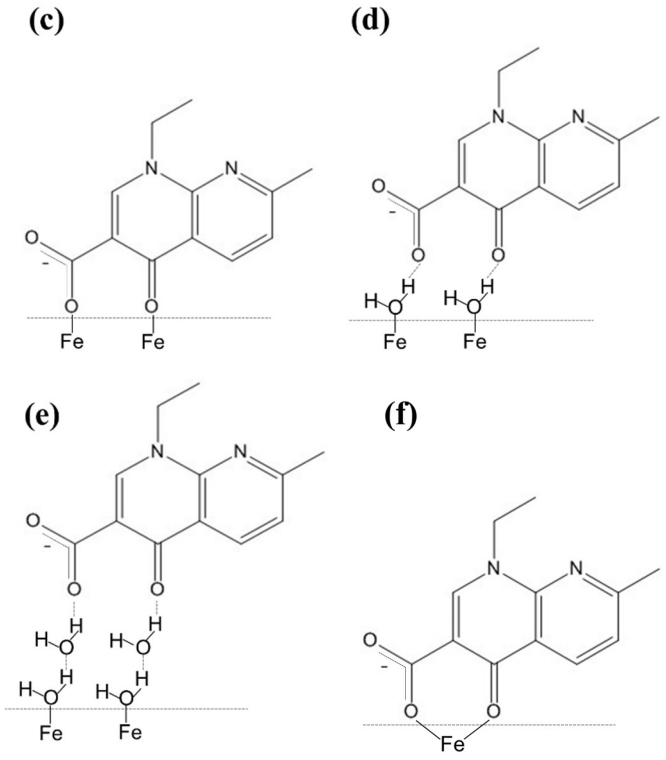

228

229 **Figure 1.** NA removal from solution for $[NA]_{tot}$ = 10 μM on 50 m^2/L of (a) goethite and (b) akaganéite versus
230 pH in 10 mM NaCl at 25 °C. The corresponding percentage of NA removal at the plateau is also given. Lines
231 are model predictions for metal-bound (MB), hydrogen-bound (HB) and outer-sphere (OS) complexes. (c)
232 MB (d) HB (e) OS of NA at goethite (001)/(101)/(210) and akaganeité (001)/(100) surfaces, and (f) MB of
233 NA at akaganeité (010) surface.

234

235 NA adsorption follows the typically expected anion adsorption envelopes for quinolones.[23,
236 25] Here, surface loadings were highest in acidic to circumneutral pH, and substantially lower
237 under alkaline conditions (Figure 1a). This can be explained by the increased electrostatic
238 repulsion between the deprotonated NA^- (pKa = 6.1) species and negatively-charged mineral
239 surface sites.

240 The ATR-FTIR spectra of NA bonded on goethite surfaces at different pH values showed

241 that the carbonyl group of bound NA was blue-shifted, and Δν (Δν = $\nu_{COO,as} - \nu_{COO,s}$)[51, 52]
242 increased upon binding compared to the unbound NA (Text S4 and Figure S4a). Accordingly,
243 the predominant NA binding mechanisms on goethite could involve the ketone group and one
244 oxygen of the carboxylate group to (singly-coordinated) -OH groups of goethite.[24, 25]. This
245 enables us to propose different surface complexes all involving carbonyl and carboxylic groups,
246 in which -OH groups of goethite may or may not be of the same Fe(III) octahedron.[53] They
247 include metal-bound (MB) complex with surface Fe sites, hydrogen-bound (HB) complex
248 (surface hydration shared ion pair) with surface hydroxo groups and outer-sphere (OS) complex
249 (solvent-surface hydration-separated ion pair) with protonated singly coordinated sites
250 ($\equiv FeOH_2^{+0.5}$). The structures of the MB, HB, and OS surface complexes are shown in Figure
251 1c-e, assuming the participation of two Fe(III) octahedra. These can be expressed through the
252 following reactions (Table 1):

253 $$2 \equiv FeOH^{-0.5} + 2\ H^+ + NA^- \rightleftharpoons (\equiv Fe)_2(NA)^0 + 2\ H_2O;\ \log K_{MB} \quad (1)$$

254 $$2 \equiv FeOH^{-0.5} + 2\ H^+ + NA^- \rightleftharpoons (\equiv FeOH_2)_2^{+\cdots}NA^-;\ \log K_{HB/OS} \quad (2)$$

255 These reactions show similar stoichiometries but the charge distribution between 0-, 1-, and 2-
256 planes differ depending on the position of NA at the mineral-water interface. In addition, at high
257 NA loadings, a NA-NA dimer is formed through intermolecular interactions, in which the
258 charge of one NA is located at the 0-plane, and the second one at the 1-plane:[25]

259 $$2 \equiv FeOH^{-0.5} + 2\ H^+ + 2\ NA^- \rightleftharpoons (\equiv FeNA)_2^- + 2\ H_2O;\ \log K_{dimer} \quad (3)$$

260 NA adsorption on akaganéite was greater than that on goethite. At pH <7, ~100% of NA
261 sorbed onto akaganéite, while the maximum NA uptake on goethite was only ~84% (Figure 1b).

We attribute this mineral-dependent adsorption to the larger (i) pH window for a positive surface charge and (ii) reactive sites on akaganéite. The larger pH window for a positive charge stems from the higher point-of-zero charge of akaganéite (9.6−10), compared to goethite (9.1−9.4). [33, 54] The higher reactivity of akaganéite can be also explained by the occurrence of reactive geminal $\equiv Fe(OH_2)_2^+$ groups at the (010) plane, which are known to have strong affinities for anionic species.[35-37]

Based on previous crystallographic considerations and spectroscopic investigations,[23] surface complexes on the (001)/(100) planes of akaganéite are expected to be comparable to those on the goethite (001)/(101) and (210) planes.[23] Therefore, the model for the (001)/(100) planes of akaganéite includes the above surface reactions (eqs.1-3), i.e. bridging metal-bound, hydrogen-bound complexes as well as a dimer. Additionally, to account for NA binding with geminal $\equiv Fe(OH_2)_2^+$ groups at the (010) plane, a monocuclear six-membered chelate complex was used, as follows (Figure 1f):

$$\equiv Fe(OH_2)(OH) + H^+ + NA^- \rightleftharpoons \equiv Fe(NA) + 2H_2O;\ \log K_{(010)} \quad (4)$$

Surface complexation reactions and their corresponding constants for NA (Table 1) provide insights into the pH-dependent behavior of NA loadings on goethite and akaganéite. NA surface speciation on goethite suggests a predominance of MB complexes under acidic pH conditions (Figure 1a) and a predominance of HB and OS complexes at high pH. In the case of akaganéite, MB complexes are found to be the prominent species at all pH values for low NA loading (10 μM), primarily associated with the binding on the (010) plane (Figure 1). However, at high NA loading (100 μM), the NA-NA dimer becomes the predominant species (Figure S5a). Moreover,

NaCl concentration variation (10-100 mM) exhibited negligible effect on NA adsorption, aligning with the dominance of MB complexes on the akaganéite surface (Figure S5b).

3.2 Cation-NA co-binding on goethite and Fe(II)-driven catalytic recrystallization

As in the NA-minerals binary systems, kinetic experiments revealed that Fe(II) and NA adsorption reactions reached equilibrium within 24 h (Figure S3). The presence of NA had no effect on Fe(II) adsorption (Figure S6), and loadings were unaffected by the order of NA and Fe(II) addition to the mineral suspensions (Figure S2).

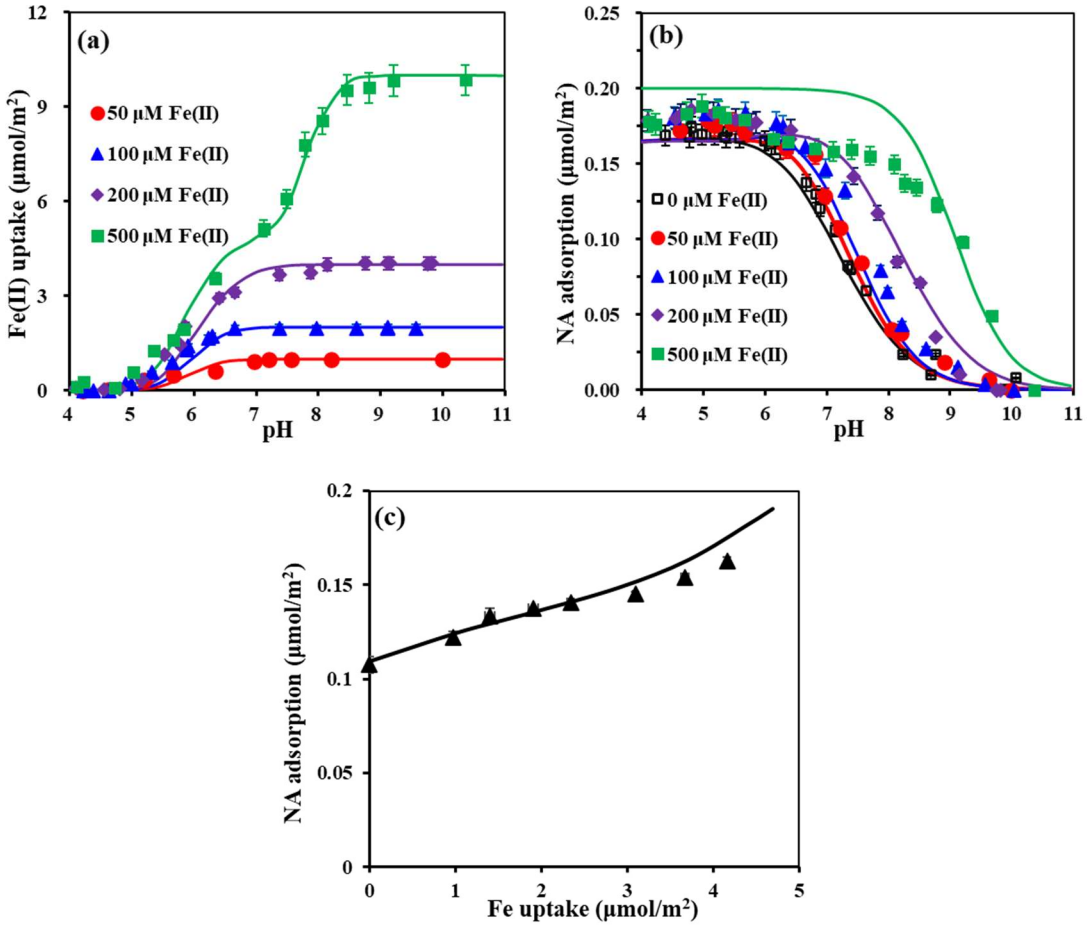

Figure 2. (a) Fe(II) and (b) NA removal from solution for$[NA]_{tot}$ = 10 µM on 50 m^2 /L goethite in 10 mM NaCl versus pH at different Fe(II) concentrations after 24 h reaction time. (c) NA adsorption versus Fe(II)

uptake. Experimental conditions: 10 μM NA and 0-500 μM Fe(II) adsorption onto 50 m^2 /L goethite in10 mM NaCl at pH = 7.1 ± 0.1. Lines are modeling results for (a) Fe(II) and (c) NA adsorption onto goethite without considering mineral transformations, (b) NA adsorption in the presence of 500 μM Fe(II) accounted for the transformation of 25% of the initial goethite into magnetite.

Fe(II) enhanced NA adsorption onto goethite at pH > 6, with no significant influence at lower pH values (Figure 2). While lower Fe(II) concentrations had only a minimal impact on NA loadings, higher concentrations (≥ 200 μM) significantly increased NA loadings and even changed the shape of the sorption edge. This observation suggests the existence of distinct mechanisms governing the (co)binding of NA and Fe(II) species. Indeed, the presence of Fe(II) could affect NA adsorption via several mechanisms. Firstly, Fe(II) can form aqueous complexes with NA:[47]

$$NA^- + Fe^{+2} \rightleftharpoons NAFe^+; \quad (5)$$

Secondly, Fe(II) can also adsorb onto goethite via the following reactions:[9, 19, 55]

$$\equiv FeOH^{-0.5} + Fe^{+2} \rightleftharpoons \equiv FeOFe^{+0.5} + H^+ \quad (6)$$

$$\equiv FeOH^{-0.5} + Fe^{+2} + H_2O \rightleftharpoons \equiv FeOFeOH^{-0.5} + 2H^+ \quad (7)$$

Here, the charge of the sorbed Fe(II) is located at the 0-plane. At the same time, alkaline conditions favored Fe(II) precipitation as $Fe(OH)_{2(s)}$ (Figure S7). Eqs. 6-7, alongside precipitation, fully accounted for the pH-dependent uptake of Fe(II) onto goethite (Figure 2a). As a result, a change in the adsorption curve shape was observed at high amount of Fe(II) (500 μM) and at pH around pH 7, which can be attributed to the precipitation of $Fe(OH)_{2(s)}$.

316 Finally, to account for the enhanced NA binding in the presence of Fe(II), a ternary
317 goethite−Fe(II)−NA complex was included in the model:
318 $2{\equiv}FeOH^{-0.5} + Fe^{+2} + NA^{-} \rightleftharpoons (\equiv FeOH)_2FeNA$ (8)
319 Our model successfully predicts NA binding to goethite at total loadings in the range of 50-200
320 μM Fe(II), by locating charges of Fe(II) and NA at the 0 plane. This is consistent with zeta
321 potential variation of goethite surface upon addition of Fe(II) or NA or both Fe(II) and NA
322 (Figure S8). For instance, addition of Fe(II) or Fe(II) and NA shifts the zeta potential towards
323 more positive values, creating a favorable condition for NA adsorption through ternary surface
324 complexation. Accounting for the electron transfer process between sorbed Fe(II) and Fe(III)
325 in goethite did not improve the modeling, as previously observed.[19]
326 The effectiveness of the optimized model parameters for Fe(II) and NA adsorption was
327 validated by successfully predicting the co-adsorption of Fe(II) and NA at pH 7 (Figure 2c).
328 This model accurately predicted an increase in NA loadings associated with Fe(II) uptake, thus
329 providing further validation for including a ternary complex in the model. However, the model
330 tended to overestimate NA binding at a higher Fe(II) concentration (500 μM) (Figure S9a).
331 Based on XRD analysis (Figure 3), we observed that Fe(II) at concentrations of 200 and 500
332 μM catalytically recrystallized goethite to magnetite. This finding warranted the inclusion of
333 magnetite in the model to account for NA adsorption upon mineral transformations.
334

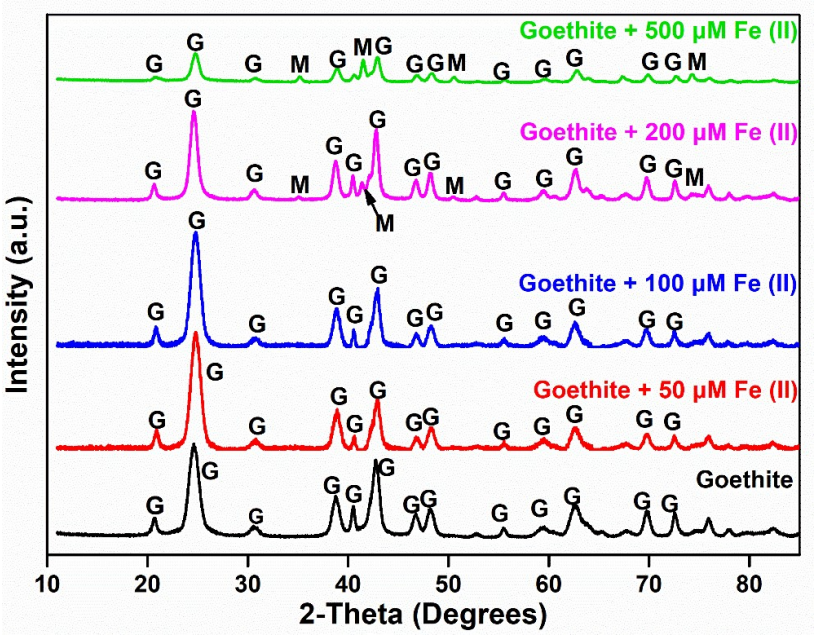

Figure 3. Powder XRD patterns of the transformation products of 50 m^2 /L goethite with different concentrations of Fe(II) at pH 9. Peaks are identified as goethite (G) or magnetite (M). Magnetite (PDF#79-0419) was detected at 2θ at 35.1, 41.4, 50.4 and 74.1°.

We propose that the formation of magnetite driven by Fe(II) can be attributed to a topotactic or reconstructive process resulting from the precipitation of white rust $Fe(OH)_{2(s)}$ at high pH:[56-58]

$$Fe(OH)_2 + 2\ \alpha\text{–}FeOOH \rightarrow Fe_3O_4 + 2H_2O \qquad (9)$$

Using the XRD intensity (I) ratios of the most intense magnetite (2θ = 41.4°) and goethite (2θ = 24.7°), $I_M/(I_M+I_G)$ peaks,[57] we find that 200 µM Fe(II) transformed only ~3% of goethite, whereas 500 µM Fe(II) transformed ~24% of the goethite into magnetite. Noting that after post-addition of 500 µM Fe(II), the goethite suspension contained a total of 6.2 mM Fe(III). As the maximum amount of iron in magnetite was 1.5 mM, we find that it represented 24 % of this total iron. This consequently supports the concept that all Fe(II) added to the suspension

converted to magnetite as resolved by XRD.

To describe NA binding onto goethite in the presence of 500 μM Fe(II), we imposed a 75% goethite - 25% magnetite assemblage in the model, and simulated NA binding onto this goethite-magnetite composite. We considered that NA bound to two surface hydroxy groups of magnetite, similar to goethite (Eq.1).[26] All the modeling parameters are presented in Table S1. Our best-fitting model predicted NA adsorption at high pH, where significant recrystallization and transformation occurred (Figure 2b). The overestimation of NA adsorption at pH < 8 was ascribed to the absence of goethite transformation to magnetite, which can be anticipated by the lack of $Fe(OH)_2$ precipitation (Figure S7). Therefore, at pH < 8, a model solely incorporating goethite as the mineral phase predicted consistently higher NA loadings (see e.g. Figure S9b).

Because the reaction involving Fe(II) could have also modified the reactivity of goethite surfaces towards NA binding, we investigated the effects of Cu(II) on NA adsorption onto goethite. As typically encountered for cations, Cu(II) adsorption increased with pH and concentration (Figure 4a). Since Cu(II)-goethite surface complexes have been well documented and defined based on ab initio molecular geometries and EXAFS spectroscopy,[59] we describe the pH-dependence of Cu(II) adsorption using the already reported equations of Cu(II) binding onto goethite, as listed in Table 1.[59, 60] The Cu(II) adsorption data can be accurately predicted by keeping all parameters equal to literature values (Figure 4a).[60] In addition, the model also predict the presence of Cu(II) precipitation as $Cu(OH)_2(s)$ for 200 μM Cu(II) (Figure S10).

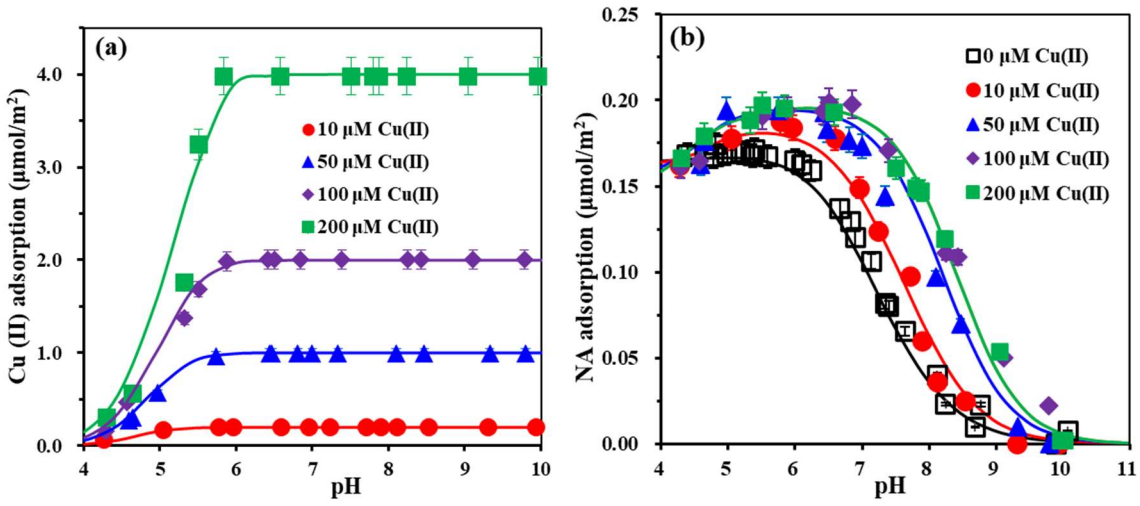

Figure 4. (a) Cu(II) and (b) NA removal from solution for $[NA]_{tot}$ = 10 µM on 50 m^2 /L goethite in 10 mM NaCl versus pH at different Cu(II) concentrations after 24 h reaction time. Lines are modeling results.

The FTIR spectra of bound NA species in the presence of Cu(II) exhibited major spectral variations for ketone and carboxyl groups compared to free NA species (Figure S4b), indicating the involvement of carboxylic and carbonyl groups of NA in the surface complexation. This is consistent with previous findings for metal complexation of quinolones,[61, 62] which reported that the most common is the bidentate coordination mode involving the carbonyl and one of the carboxylate oxygen atoms (See Figure S11 for NA-Cu(II) complex).

Accordingly, the presence of Cu(II) significantly increased NA adsorption and shifted the sorption edge to higher pH (Figure 4b). NA sorption increased sharply at Cu(II) concentrations of less than 100 µM, while larger concentrations did not have any significantly higher impacts on loadings. As ternary surface-cation-ligand complexes generally enhance ligand binding by cations,[27, 41, 60, 63] we modeled greater NA loadings using the following reaction, with locating charges of Cu(II) and NA at the 0 plane:

$$2{\equiv}FeOH^{-0.5} + NA^{-} + Cu^{+2} \rightleftharpoons ({\equiv}FeOH)_2CuNA \quad (10)$$

This ternary complexation is also consistent with the zeta potential variation of goethite surface, where the excess positive charges induced by the adsorption of Cu(II) may favor the adsorption of negative NA species, and thus the formation of goethite-Cu(II)-NA ternary complexes (Figure S8). The difference in the influence of Cu(II) and Fe(II) on NA sorption can be also related to the hard/soft acids/bases (HSABs) principle.[64] NA^- and OH^- are hard bases, while Cu(II) and Fe(II) are hard acids, with Fe(II) being the harder one. As such, the interaction is stronger in the bond of Cu(II)−OH/ Cu(II)−NA than that of Fe(II)−OH/ Fe(II)−NA, [47, 64] which explains the higher adsorption of NA in the presence of Cu(II) compared to Fe(II).

To further interpret the NA adsorption in the presence of 100 and 200 μM Cu(II), we compared the surface species distribution of NA and Cu(II) (Figure S12). The increase in Cu(II) concentration from 100 to 200 μM resulted in a significant increase in goethite-Cu(II) complex and $Cu(OH)_2$ precipitation. However, the amount of the goethite-Cu(II)-NA ternary complex was very similar under these two Cu(II) concentrations. This falls in line with our experimental findings where 100 μM Cu(II) and 200 μM Cu(II) induced the same NA sorbed amount, corresponding to 100 % adsorption of initial added NA (10 μM). This model consequently contributes to a mounting body of evidence for the importance of ternary surface complexation in accounting for the binding of metal cations and quinolone antibiotics at goethite surfaces.[27, 41]

3.3 Cation-NA co-binding on akaganéite and Fe(II)-driven catalytic recrystallization

In contrast to the case of goethite, adsorption of Fe(II) from akaganéite suspensions

406 containing both Fe(II) and NA had marginal effects on NA loadings (Figures 5 and S13). As
407 XRD (Figure 6) also revealed that no mineralogical transformations occurred at low Fe(II)
408 concentrations, we modelled Fe(II) and NA binding using the same modeling strategy for
409 predicting adsorption (Figure S14 and Text S3). Our model explains the insensitivity of NA
410 loadings to 50-100 μM Fe(II), as the competition of Fe(II) for NA adsorption counteracts the
411 enhancement in adsorption associated with ternary complexation. The model also predicts that
412 the higher Fe(II) surface loadings were achieved in solutions of larger Fe(II) concentrations
413 and/or higher pH.
414

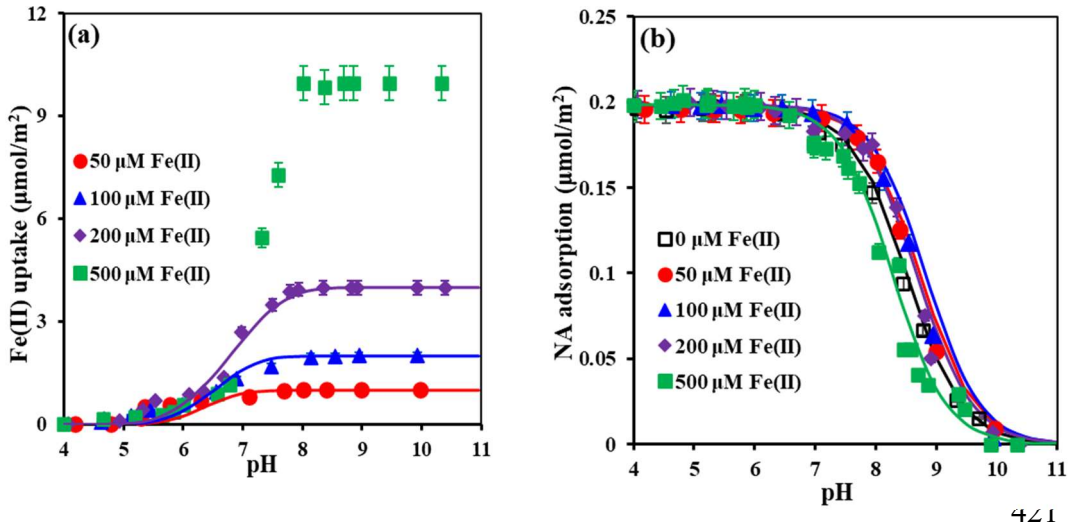

421

422 **Figure 5.** (a) Fe(II) and (b) NA removal from solution for $[NA]_{tot}$ = 10 μM on 50 m^2 /L akaganéite in 10 mM
423 NaCl versus pH at different Fe(II) concentrations after 24 h reaction time. Lines are modeling results. The
424 NA adsorption modeling result in the presence of 200 μM Fe(II) and 500 μM Fe(II) accounted for the
425 transformation of the initial akageneite into 100% goethite, and into 50% goethite and 50% magnetite,
426 respectively. Because of greater akaganéite transformation at 500 μM Fe(II), the corresponding Fe(II) uptake
427 was not modeled.

Based on XRD analysis (Figure 6), we also observed that akaganéite underwent recrystallization into goethite when exposed to 200 μM Fe(II), while in the presence of 500 μM Fe(II), it transformed into both goethite and magnetite. From the intensity ratios of the most intense XRD peaks of the respective minerals, we find that ~52 % goethite and ~48 % magnetite were formed after exposing akaganéite to 500 μM Fe(II). Interestingly, the proportion of magnetite formed (48%) closely matched the Fe(II) reacted to the Fe(III) content of akaganétite (42%). As goethite was found as the final product of akaganéite in the presence of 200 μM Fe(II), we used our previously established NA-goethite surface complexation model to predict NA adsorption. Our best fitting of the adsorption curve required an increasing of the NA-goethite surface complex constant by only 1.2 log K units. This suggests that the newly formed goethite exhibits a higher capacity for NA adsorption.

To account for the akaganéite transformation in the presence of 500 μM Fe(II), we adapted our NA surface complexation model to include a 50% goethite - 50% magnetite composite (Table S1). Notably, the updated model successfully predicted NA adsorption in the presence of 500 μM Fe(II) across all pH values (Figure 5b and S15). It is worth noting that the resulting magnetite exhibited distinct surface properties and reactivity towards NA adsorption as compared to previous experiments, as it strongly depends on the type of ferric precursor (goethite or akageneite).[58]

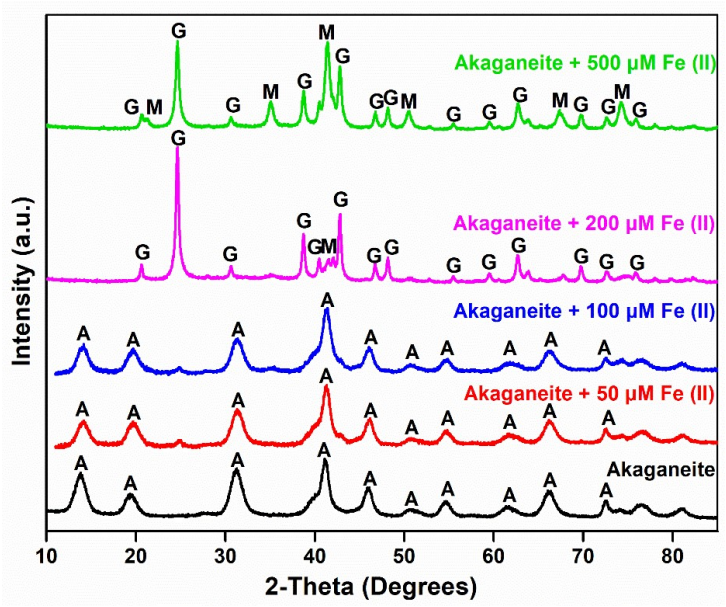

447

448 **Figure 6.** Powder XRD patterns of the transformation products of 50 m^2 /L akaganéite with different

449 concentrations of Fe(II) at pH 9. A, G and M refer to peaks of akaganéite, goethite and magnetite, respectively.

450

451

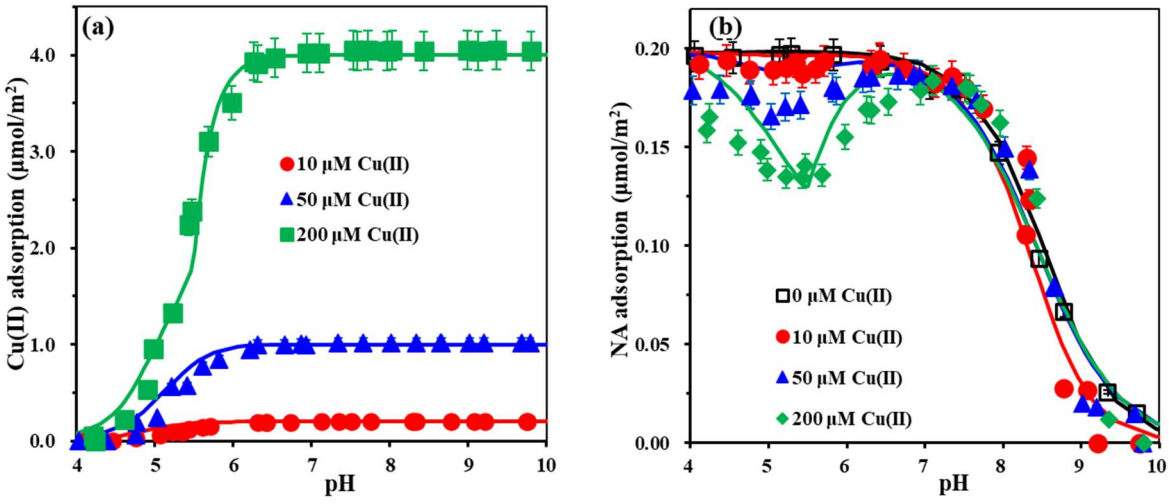

452

453 **Figure 7.** (a) Cu(II) and (b) NA removal from solution for$[NA]_{tot}$ = 10 µM on 50 m^2 /L akaganéite in 10 mM

454 NaCl versus pH at different Cu(II) concentrations after 24 h reaction time. Lines are modeling results.

455

As in the case of goethite, we also investigated the role that Cu(II) species could play on NA binding onto akaganéite. The results revealed that Cu(II) exerted a significant inhibitory effect on NA adsorption under acidic pH conditions, with the extent of inhibition increasing with higher Cu(II) concentrations (Figure 7b). Previous spectroscopic studies and theoretical calculations indicated that Cu(II) forms bidentate and tridentate inner-sphere complexes with the (100)/(001) planes of akaganéite.[59] These can be expressed as:

$$2{\equiv}FeOH^{-0.5} + Cu^{+2} \rightleftharpoons ({\equiv}FeOH)_2Cu^{+} \quad (11)$$

$$3{\equiv}FeOH^{-0.5} + 2\ Cu^{+2} + 2\ H_2O \rightleftharpoons ({\equiv}FeOH)_3Cu_2^{+0.5} + 2H^{+} \quad (12)$$

Although these added reactions (Table 1) effectively predicted Cu(II) loadings (Figure S16a), the model overestimated NA loadings at low pH (Figure S16b). As an attempt to improve this model, we introduced competitive Cu(II) binding reactions with the sites of the (010) plane:

$${\equiv}Fe(OH_2)OH^{0} + Cu^{+2} \rightleftharpoons ({\equiv}FeOCu)OH + 2H^{+} \quad (13)$$

While this reaction had limited NA-akaganéite loadings (Figure 1b), it still underestimated NA adsorption in the presence of Cu(II) (Figure S16c). In contrast, incorporating an akaganéite-Cu(II)-NA ternary complex into the model, as we did for goethite, and locating the charges of Cu(II) and NA at the 0 plane and 1 plane, respectively (Table 1), made a considerable improvement in the modeling predictions (Figure 7b). This improvement was observed even at larger NA concentration (100 μM) in the presence of 100-200 μM Cu(II) (Figure S17). Although there was no overall increase in total amount of sorbed NA observed in presence of Cu(II) at high pH values, the modeling data suggests a significant role of ternary surface complexation in NA binding onto akaganéite surfaces. Unlike goethite, where both NA and

Cu(II) bind to the same planes, our model suggests that NA preferentially targets the (010) planes while Cu(II) predominantly binds to the (100)/(001) planes, leading to the formation of ternary complex at the (100)/(001) planes (Figure 8a).

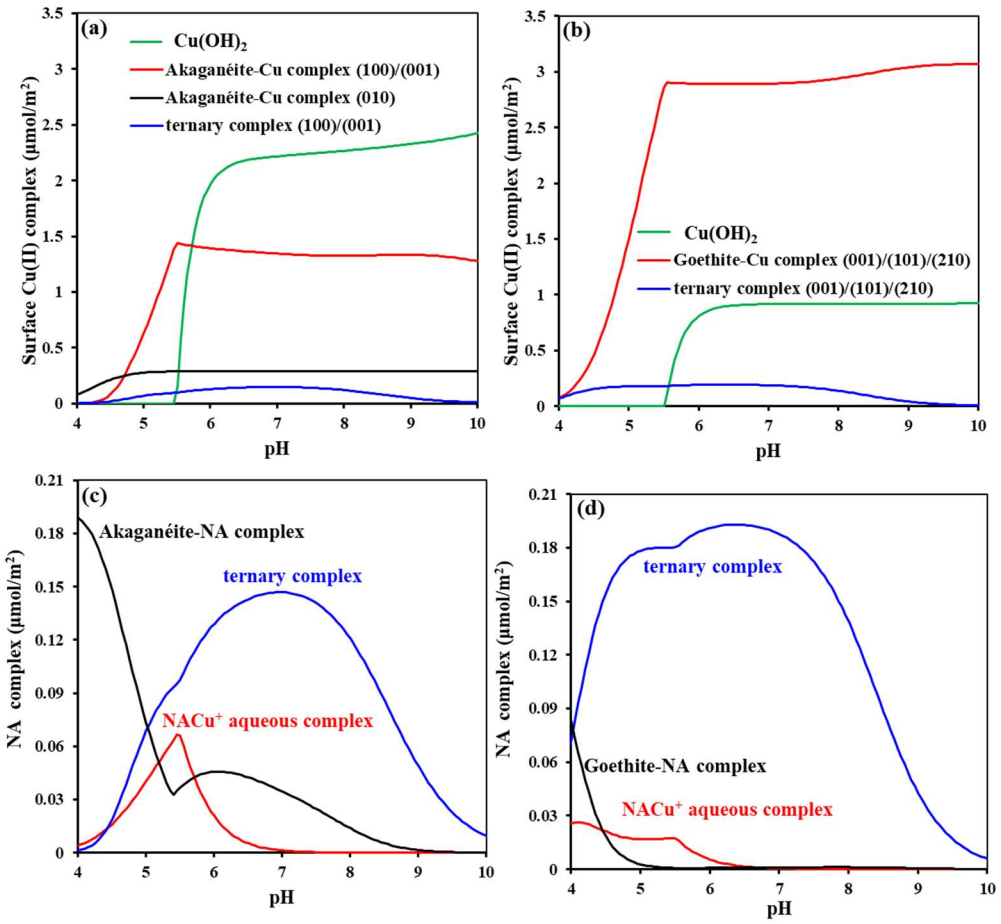

Figure 8. Modeling results of different surface species. 10 μM NA and 200 μM Cu(II) adsorption onto 50 m^2 /L (a, c) akaganéite and (b, d) goethite in 10 mM NaCl versus pH after 24 h reaction time. Surface Cu(II) complex on (a) akaganéite and (b) goethite. NA complex in the presence of (c) akaganéite and (d) goethite.

To gain further insights into the mineral-dependent effect of Cu(II), we compared the surface distribution of Cu(II) complex between the two minerals in the presence of 200 μM Cu(II) (Figure 8). Despite similar Cu(II) uptake was observed on both minerals, there was clear difference in surface speciation. The akaganéite mineral demonstrated a significantly higher

amount of $Cu(OH)_2$ precipitate compared to goethite, whereas the ternary complex on akaganéite was much lower in comparison to goethite (Figure 8a,b). In addition, the $NACu^+$ aqueous complex was much larger in the presence of akaganéite (Figure 8c,d), which could potentially explain the decreased NA binding onto akaganéite in the presence of Cu(II) at low pH values.

4. ENVIRONMENTAL IMPLICATIONS

Through batch adsorption experiments, surface complexation modeling, ATR-FTIR and XRD analysis, we have discovered that the co-binding of NA with cations (Fe(II) or Cu(II)) is strongly affected by pH, cation concentration and FeOOH phase. Furthermore, we also find that the type of ternary complexation is strongly linked to the nature of the intervening cation and mineral surface structure.

These findings have important implications for understanding the fate of quinolone antibiotics in environments containing Fe(II) and Cu(II) and FeOOH, such as oxic-anoxic boundaries in marine and freshwater basins, oxycline in sediments, and sediment−water interfaces. For instance, Cu(II), commonly used as fungicide, could also have contrasting effects by decreasing the affinity of quinolone antibiotics for akaganéite while increasing their affinity for goethite. Additionally, Fe(II) produced through microbial respiration and weathering of Fe(II)-bearing minerals, could have a considerable impact on quinolone antibiotics binding on Fe(III) (oxyhydr)oxide minerals via ternary complexation and/or mineralogical transformation. In addition to Cu(II) and Fe(II), other cations such as Ca(II),[65] Zn(II),[66] Pb(II),[67] Cd(II)[68] and Ni(II)[69] would also influence the adsorption of organic compounds through ternary

surface complexation. Given the prevalence of mineral-cation-ligand ternary complexes, we propose that the intriguing phenomenon observed in this study extends beyond NA and can be generalized to other organic pollutants containing carboxyl and carbonyl functional groups.

Considering that FeOOH-bound Fe(II) plays an important role in redox-driven transformations occurring in natural environments, this study provides valuable insights that can help guide future research on the fate of redox-active organic contaminants in heterogeneous natural systems. Additionally, the transformation of Fe(III) oxy(hydr)oxides into magnetite can occur upon exposure to Fe(II) at alkaline conditions, and the resulting magnetite may exhibit varying reactivity depending on the ferric precursor. For example, magnetite formed from akaganéite appears to possess higher reactivity compared to that derived from goethite. These findings have thus important implications for better understanding the natural attenuation of contaminants under reducing conditions, and/or the development of magnetite-based remediation technologies. Future studies should explore Fe(II)-induced mineral transformations as well as mineral-cation-ligand ternary interactions under real-world conditions of water flow and natural chemical constituents.

SUPPORTING INFORMATION

Synthesis and characterization of goethite and akaganéite particles; ATR-FTIR investigations and surface complexation modeling; Crystal planes and site densities of minerals and modeling parameters; Zeta potentials of goethite and akaganéite; Kinetics data of Fe(II) and NA adsorption onto minerals; Additional adsorption data of NA and/or Cu versus pH and NaCl

concentrations in single and binary systems; Additional experimental and modeling data on Cu adsorption and precipitation, NA adsorbed species distribution under different Cu(II) or Fe(II) concentrations, and NA adsorption on magnetite, akaganéite, goethite, and goethite/magnetite composite.

ACKNOWLEDGMENTS

We gratefully thank the Natural Science Foundations of China (NSFC22006165), the Fundamental Research Funds for the Central Universities (CZQ21012), the Swedish Research Council (2020-04853), and the CNRS (IRP CHEMICY, 2023-2027).

Table 1. Surface Complexation Model

Aqueous solutions	log K				ref
$NAH_{(S)} \rightleftharpoons NAH_{(aq)}$	-4.0				[25]
$NA^- + H^+ \rightleftharpoons NAH$	6.19				[25]
$Fe^{+2} + NA^- \rightleftharpoons FeNA^+$	3.99				[47]
$NA^- + Cu^{2+} \rightleftharpoons NACu^+$	6.155				[47]
Goethite[a]	**log K**	**Δz_0**	**Δz_1**	**Δz_2**	**ref**
$2 \equiv FeOH^{-0.5} + 2H^+ + NA^- \rightleftharpoons (\equiv Fe)_2(NA)^0 + 2H_2O$	20.2±0.1	+1	0	0	[25]
$2 \equiv FeOH^{-0.5} + 2H^+ + NA^- \rightleftharpoons (\equiv FeOH_2)_2^+ \cdots NA^-$	19.8±0.1	+2	-1	0	[25]
$2 \equiv FeOH^{-0.5} + 2H^+ + NA^- \rightleftharpoons (\equiv FeOH_2)_2^+ \cdots NA^-$	20.9±0.1	+2	0	-1	[25]
$2 \equiv FeOH^{-0.5} + 2H^+ + 2NA^- \rightleftharpoons (\equiv Fe)_2(NA)^0 \cdots NA^-$	22.2±0.1	+1	-1	0	[25]
$\equiv FeOH^{-0.5} + Fe^{+2} \rightleftharpoons \equiv FeOFe^{+0.5} + H^+$	1.3±0.1	+1	0	0	[19]
$\equiv FeOH^{-0.5} + Fe^{+2} + H_2O \rightleftharpoons \equiv FeOFeOH^{-0.5} + 2H^+$	-11.3±0.1	0	0	0	[19]
$2 \equiv FeOH^{-0.5} + Fe^{+2} + NA^- \rightleftharpoons (\equiv FeOH)_2FeNA$	13±0.2	+10	0	0	This study
$2\equiv FeOH^{-0.5} + Cu^{+2} \rightleftharpoons (\equiv FeOH)_2Cu^+$	9.18	0.84	1.16	0	[60]
$2\equiv FeOH^{-0.5} + Cu^{+2} + H_2O \rightleftharpoons (\equiv FeOH)_2CuOH + H^+$	3.6	0.84	0.16	0	[60]
$2\equiv FeOH^{-0.5} + 2\ Cu^{+2} + 2H_2O \rightleftharpoons (\equiv FeOH)_2Cu_2(OH)_2^+ + 2H^+$	3.65	0.84	1.16	0	[60]
$2\equiv FeOH^{-0.5} + 2\ Cu^{+2} + 3H_2O \rightleftharpoons (\equiv FeOH)_2Cu_2(OH)_3 + 3H^+$	-3.1	0.84	0.16	0	[60]
$2\equiv FeOH^{-0.5} + NA^- + Cu^{+2} \rightleftharpoons (\equiv FeOH)_2CuNA$	16.25±0.1	1	0	0	This study
Akaganéite[b]	**log K**	**Δz_0**	**Δz_1**	**Δz_2**	**ref**
$2 \equiv FeOH^{-0.5} + 2H^+ + NA^- \rightleftharpoons (\equiv Fe)_2(NA)^0 + 2H_2O$	20.6±0.2	+1	0	0	This study
$2 \equiv FeOH^{-0.5} + 2H^+ + NA^- \rightleftharpoons (\equiv FeOH_2)_2^+ \cdots NA^-$	20.6±0.1	+2	-1	0	This study
$\equiv Fe(OH_2)(OH)^0 + H^+ + NA^- \rightleftharpoons \equiv Fe\ (NA)^0 + 2H_2O$	13.4 ± 0.1	0	0	0	This study
$2\equiv FeOH^{-0.5} + 2\ H^+ + 2\ NA^- \rightleftharpoons (\equiv FeNA)_2^- + 2\ H_2O$	25.3 ± 0.1	1	-1	0	This study
$\equiv FeOH^{-0.5} + Fe^{+2} \rightleftharpoons \equiv FeOHFe^{+1.5}$	0.85±0.08	+2	0	0	This study
$\equiv FeOH^{-0.5} + Fe^{+2} + H_2O \rightleftharpoons \equiv FeOFeOH^{-0.5} + 2H^+$	-17.2±0.1	0	0	0	This study
$2 \equiv FeOH^{-0.5} + Fe^{+2} + NA^- \rightleftharpoons (\equiv FeOH)_2FeNA$	13.7±0.2	1	0	0	This study
$2\equiv FeOH^{-0.5} + Cu^{+2} \rightleftharpoons (\equiv FeOH)_2Cu^+$	insensitive	2	0	0	[59]
$3\equiv FeOH^{-0.5} + 2\ Cu^{+2} + 2\ H_2O \rightleftharpoons (\equiv FeOH)_3Cu_2^{+0.5} + 2H^+$	6.56±0.1	2	0	0	[59]
$\equiv Fe(OH_2)OH^0 + Cu^{+2} \rightleftharpoons (\equiv FeOCu)OH + 2H^+$	-4±0.1	0	0	0	This study
$2\equiv FeOH^{-0.5} + NA^- + Cu^{+2} \rightleftharpoons (\equiv FeOH)_2CuNA$	16.2±0.1	2	-1	0	This study

[a]TPM with C_1= 2.3 F/m^2 and C_2=1.07 F/m^2; Site densities: [$\equiv FeOH^{-0.5}$] = 3.12 sites nm^{-2} and [$\equiv Fe_3O^{-0.5}$] = 3.12 sites nm^{-2} on (001)/(101) planes (90 % of the surface area), and [$\equiv FeOH^{-0.5}$] = 7.4 sites nm^{-2} on (210) plane (10 % of the surface area).

[b]TPM with C_1= 2.3 F/m^2 and C_2=1.6 F/m^2. [$\equiv FeOH^{-0.5}$] = 3.09 sites nm^{-2}, [$\equiv Fe_2OH$]=3.09 sites nm^{-2}, [$\equiv Fe_3O_I^{-0.5}$] = 6.18 sites nm^{-2}, [$\equiv Fe_3O_{II}^{-0.5}$] = 3.09 sites nm^{-2}on (001)/(100) planes (95% of the surface area), and [$\equiv Fe_2OH$] = 7.06 sites nm^{-2} and [$\equiv Fe(OH_2)_2$] = 3.53 sites nm^{-2}on (010) plane (5% of the surface area)

REFERENCE

1. Xiu, W.; Yuan, W. J.; Polya, D. A.; Guo, H. M.; Lloyd, J. R., A critical review of abiotic and microbially-mediated chemical reduction rates of Fe(III) (oxyhydr)oxides using a reactivity model. *Applied Geochemistry* **2021,** *126*, 104895.
2. Huang, J. Z.; Jones, A.; Waite, T. D.; Chen, Y. L.; Huang, X. P.; Rosso, K. M.; Kappler, A.; Mansor, M.; Tratnyek, P. G.; Zhang, H. C., Fe(II) Redox Chemistry in the Environment. *Chemical Reviews* **2021,** *121*, (13), 8161-8233.
3. Frierdich, A. J.; Helgeson, M.; Liu, C.; Wang, C.; Rosso, K. M.; Scherer, M. M., Iron Atom Exchange between Hematite and Aqueous Fe(II). *Environ. Sci. Technol.* **2015,** *49*, (14), 8479-8486.
4. Gorski, C. A.; Handler, R. M.; Beard, B. L.; Pasakarnis, T.; Johnson, C. M.; Scherer, M. M., Fe Atom Exchange between Aqueous Fe2+ and Magnetite. *Environ. Sci. Technol.* **2012,** *46*, (22), 12399-12407.
5. Handler, R. M.; Frierdich, A. J.; Johnson, C. M.; Rosso, K. M.; Beard, B. L.; Wang, C. M.; Latta, D. E.; Neumann, A.; Pasakarnis, T.; Premaratne, W. A. P. J.; Scherer, M. M., Fe(II)-Catalyzed Recrystallization of Goethite Revisited. *Environ. Sci. Technol.* **2014,** *48*, (19), 11302-11311.
6. Boland, D. D.; Collins, R. N.; Glover, C. J.; Payne, T. E.; Waite, T. D., Reduction of U(VI) by Fe(II) during the Fe(II)-Accelerated Transformation of Ferrihydrite. *Environ. Sci. Technol.* **2014,** *48*, (16), 9086-9093.
7. Catalano, J. G.; Luo, Y.; Otemuyiwa, B., Effect of Aqueous Fe(II) on Arsenate Sorption on Goethite and Hematite. *Environ. Sci. Technol.* **2011,** *45*, (20), 8826-8833.
8. Frierdich, A. J.; Luo, Y.; Catalano, J. G., Trace element cycling through iron oxide minerals during redox-driven dynamic recrystallization. *Geology* **2011,** *39*, (11), 1083-1086.
9. Huang, J. Z.; Wang, Q. H.; Wang, Z. M.; Zhang, H. C., Interactions and Reductive Reactivity in Ternary Mixtures of Fe(II), Goethite, and Phthalic Acid Based on a Combined Experimental and Modeling Approach. *Langmuir* **2019,** *35*, (25), 8220-8227.
10. Hansel, C. M.; Benner, S. G.; Fendorf, S., Competing Fe(II)-Induced Mineralization Pathways of Ferrihydrite. *Environ. Sci. Technol.* **2005,** *39*, (18), 7147-7153.
11. Pedersen, H. D.; Postma, D.; Jakobsen, R.; Larsen, O., Fast transformation of iron oxyhydroxides by the catalytic action of aqueous Fe(II). *Geochimica et Cosmochimica Acta* **2005,** *69*, (16), 3967-3977.
12. Yang, L.; Steefel, C. I.; Marcus, M. A.; Bargar, J. R., Kinetics of Fe(II)-Catalyzed Transformation of 6-line Ferrihydrite under Anaerobic Flow Conditions. *Environ. Sci. Technol.* **2010,** *44*, (14), 5469-5475.
13. Handler, R. M. B., B. L.; Johnson, C. M.; Scherer, M. M, Atom Exchange between Aqueous Fe(II) and Goethite: An Fe Isotope Tracer Study. *Environ. Sci. Technol.* **2009**, *43*, 1102–1107.
14. Hu, Y.; Xue, Q.; Tang, J.; Fan, X.; Chen, H. H., New insights on Cr(VI) retention by ferrihydrite in the presence of Fe(II). *Chemosphere* **2019,** *222*, 511-516.
15. Hao, T. W.; Huang, Y.; Li, F. B.; Wu, Y. D.; Fang, L. P., Facet-dependent Fe(II) redox chemistry on iron oxide for organic pollutant transformation and mechanisms. *Water Research* **2022,** *219*, 118587.
16. Cárdenas-Hernández, P. A.; Anderson, K. A.; Murillo-Gelvez, J.; Di Toro, D. M.; Allen, H. E.; Carbonaro, R. F.; Chiu, P. C., Reduction of 3-Nitro-1,2,4-Triazol-5-One (NTO) by the Hematite–Aqueous Fe(II) Redox Couple. *Environ. Sci. Technol.* **2020,** *54*, (19), 12191-12201.
17. Orsetti, S.; Laskov, C.; Haderlein, S. B., Electron Transfer between Iron Minerals and Quinones: Estimating the Reduction Potential of the Fe(II)-Goethite Surface from AQDS Speciation. *Environ. Sci. Technol.* **2013,** *47*, (24), 14161-14168.
18. Silvester, E.; Charlet, L.; Tournassat, C.; Gé hin, A.; Gren è che, J.-M.; Liger, E., Redox potential measurements and Mössbauer spectrometry of FeII adsorbed onto FeIII (oxyhydr)oxides. *Geochimica et Cosmochimica Acta* **2005,** *69*, (20), 4801-4815.
19. Hinkle, M. A. G.; Wang, Z. M.; Giammar, D. E.; Catalano, J. G., Interaction of Fe(II) with phosphate and sulfate on iron oxide surfaces. *Geochimica Et Cosmochimica Acta* **2015,** *158*, 130-146.
20. Ardo, S. G.; Nelieu, S.; Ona-Nguema, G.; Delarue, G.; Brest, J.; Pironin, E.; Morin, G., Oxidative degradation of nalidixic acid by nano-magnetite via Fe2+/O2-mediated reactions. *Environ Sci Technol* **2015,** *49*, (7), 4506-4514.
21. Lorphensri, O.; Intravijit, J.; Sabatini, D. A.; Kibbey, T. C.; Osathaphan, K.; Saiwan, C., Sorption of acetaminophen, 17alpha-ethynyl estradiol, nalidixic acid, and norfloxacin to silica, alumina. and a hydrophobic medium. *Water Res* **2006,** *40*, (7), 1481-1491.
22. Kovalakova, P.; Cizmas, L.; McDonald, T. J.; Marsalek, B.; Feng, M. B.; Sharma, V. K., Occurrence and toxicity of antibiotics in the aquatic environment: A review. *Chemosphere* **2020,** *251*, 126351.
23. Marsac, R.; Martin, S.; Boily, J. F.; Hanna, K., Oxolinic Acid Binding at Goethite and Akaganeite Surfaces: Experimental Study and Modeling. *Environ. Sci. Technol.* **2016,** *50*, (2), 660-668.

24. Xu, J.; Marsac, R.; Costa, D.; Cheng, W.; Wu, F.; Boily, J. F.; Hanna, K., Co-Binding of Pharmaceutical Compounds at Mineral Surfaces: Molecular Investigations of Dimer Formation at Goethite/Water Interfaces. *Environ. Sci. Technol.* **2017,** *51*, (15), 8343-8349.
25. Xu, J.; Marsac, R.; Wei, C.; Wu, F.; Boily, J. F.; Hanna, K., Cobinding of Pharmaceutical Compounds at Mineral Surfaces: Mechanistic Modeling of Binding and Cobinding of Nalidixic Acid and Niflumic Acid at Goethite Surfaces. *Environ. Sci. Technol.* **2017,** *51*, (20), 11617-11624.
26. Cheng, W.; Marsac, R.; Hanna, K., Influence of Magnetite Stoichiometry on the Binding of Emerging Organic Contaminants. *Environ. Sci. Technol.* **2018,** *52*, (2), 467-473.
27. Cheng, W.; Kalahroodi, E. L.; Marsac, R.; Hanna, K., Adsorption of Quinolone Antibiotics to Goethite under Seawater Conditions: Application of a Surface Complexation Model. *Environ. Sci. Technol.* **2019,** *53*, (3), 1130-1138.
28. Cheng, W.; Zhou, L.; Marsac, R.; Boily, J. F.; Hanna, K., Effects of organic matter-goethite interactions on reactive transport of nalidixic acid: Column study and modeling. *Environ Res* **2020,** *191*, 110187.
29. Luo, T.; Xu, J.; Cheng, W.; Zhou, L.; Marsac, R.; Wu, F.; Boily, J. F.; Hanna, K., Interactions of Anti-Inflammatory and Antibiotic Drugs at Mineral Surfaces Can Control Environmental Fate and Transport. *Environ. Sci. Technol.* **2022,** *56*, (4), 2378-2385.
30. Zhou, L.; Cheng, W.; Marsac, R.; Boily, J. F.; Hanna, K., Silicate surface coverage controls quinolone transport in saturated porous media. *J Colloid Interf Sci* **2022,** *607*, 347-356.
31. Liu, H. B.; Chen, T. H.; Frost, R. L., An overview of the role of goethite surfaces in the environment. *Chemosphere* **2014,** *103*, 1-11.
32. Rémazeilles, C.; Refait, P., On the formation of β-FeOOH (akaganéite) in chloride-containing environments. *Corrosion Science* **2007,** *49*, (2), 844-857.
33. Gaboriaud, F.; Ehrhardt, J.-J., Effects of different crystal faces on the surface charge of colloidal goethite (α-FeOOH) particles: an experimental and modeling study. *Geochimica et Cosmochimica Acta* **2003,** *67*, (5), 967-983.
34. Hanna, K.; Martin, S.; Quilès, F.; Boily, J.-F., Sorption of phthalic acid at goethite surfaces under flow-through conditions. *Langmuir : the ACS journal of surfaces and colloids* **2014,** *30 23*, 6800-6807.
35. Kozin, P. A.; Boily, J.-F., Proton Binding and Ion Exchange at the Akaganéite/Water Interface. *The Journal of Physical Chemistry C* **2013,** *117*, (12), 6409-6419.
36. Song, X.; Boily, J.-F., Competitive ligand exchange on akaganéite surfaces enriches bulk chloride loadings. *J Colloid Interf Sci* **2012,** *376*, (1), 331-333.
37. Song, X.; Boily, J.-F., Surface Hydroxyl Identity and Reactivity in Akaganéite. *The Journal of Physical Chemistry C* **2011,** *115*, (34), 17036-17045.
38. Grover, G.; Kini, S. G., Synthesis and evaluation of new quinazolone derivatives of nalidixic acid as potential antibacterial and antifungal agents. *Eur J Med Chem* **2006,** *41*, (2), 256-262.
39. Fatta-Kassinos, D.; Meriç, S.; Nikolaou, A. D., Pharmaceutical residues in environmental waters and wastewater: current state of knowledge and future research. *Analytical and Bioanalytical Chemistry* **2011,** *399*, 251-275.
40. Gothwal, R.; Shashidhar, T., Antibiotic Pollution in the Environment: A Review. *Clean - Soil, Air, Water* **2015,** *43*, (4), 479-489.
41. Gu, X. Y.; Tan, Y. Y.; Tong, F.; Gu, C., Surface complexation modeling of coadsorption of antibiotic ciprofloxacin and Cu(II) and onto goethite surfaces. *Chem Eng J* **2015,** *269*, 113-120.
42. Kong, X.; Feng, S.; Zhang, X.; Li, Y., Effects of bile salts and divalent cations on the adsorption of norfloxacin by agricultural soils. *J Environ Sci* **2014,** *26*, (4), 846-854.
43. Li, X.; Bi, E., The impacts of Cu(II) complexation on gatifloxacin adsorption onto goethite and hematite. *Journal of Environmental Quality* **2020,** *49*, (1), 50-60.
44. Vogel, A. I., Vogel's textbook of quantitative chemical analysis. In 6th ed. / ed.; Mendham, J.; Denney, R. C.; Barnes, J. D.; Thomas, M., Eds. Prentice Hall: Harlow, England, 2000.
45. Parkhurst, D. L.; Appelo, C. A. J. *User's guide to PHREEQC (Version 2): A computer program for speciation, batch-reaction, one-dimensional transport, and inverse geochemical calculations*; 99-4259; 1999.
46. Hiemstra, T.; Van Riemsdijk, W. H., A Surface Structural Approach to Ion Adsorption: The Charge Distribution (CD) Model. *J Colloid Interf Sci* **1996,** *179*, (2), 488-508.
47. Timmers, K.; Sternglanz, R., Ionization and divalent cation dissociation constants of nalidixic and oxolinic acids. *Bioinorganic Chemistry* **1978,** *9*, (2), 145-155.
48. Kinniburgh, D. G.; Cooper, D. In *PhreePlot: Creating graphical output with PHREEQC*, 2011; 2011.
49. Powell, M. J. D., A Method for Minimizing a Sum of Squares of Non-Linear Functions Without Calculating Derivatives. *The Computer Journal* **1965,** *7*, (4), 303-307.

50. Jolsterå, R.; Gunneriusson, L.; Holmgren, A., Surface complexation modeling of Fe3O4–H+ and Mg(II) sorption onto maghemite and magnetite. *J Colloid Interf Sci* **2012,** *386*, (1), 260-267.
51. Nakamoto, K., Infrared and Raman Spectra of Inorganic and Coordination Compounds. Part B: Applications in Coordination,Organometallic, and Biorganic Chemistry,. *Wiley-Interscience::New York* **2009,** 424 p.
52. Tackett, J. E., FT-IR characterization of metal acetates in aqueous solution. *Appl. Spectrosc* **1989**, 43 (3), 483.
53. Boily, J.-F.; Persson, P.; Sjöberg, S., Benzenecarboxylate surface complexation at the goethite (α-FeOOH)/water interface: II. Linking IR spectroscopic observations to mechanistic surface complexation models for phthalate, trimellitate, and pyromellitate. *Geochimica et Cosmochimica Acta* **2000,** *64*, (20), 3453-3470.
54. Lutzenkirchen., J.-F. o. B. J., Modeling proton binding at the goethite (α-FeOOH)−water. *Colloids and Surfaces A: Physicochemical and Engineering Aspects* **2001**, 179 (1), 11-27.
55. Hiemstra, T.; van Riemsdijk, W. H., Adsorption and surface oxidation of Fe(II) on metal (hydr)oxides. *Geochimica et Cosmochimica Acta* **2007,** *71*, (24), 5913-5933.
56. Ahn, T.; Kim, J. H.; Yang, H.-M.; Lee, J. W.; Kim, J.-D., Formation Pathways of Magnetite Nanoparticles by Coprecipitation Method. *The Journal of Physical Chemistry C* **2012,** *116*, (10), 6069-6076.
57. Usman, M.; Abdelmoula, M.; Faure, P.; Ruby, C.; Hanna, K., Transformation of various kinds of goethite into magnetite: Effect of chemical and surface properties. *Geoderma* **2013,** *197-198*, 9-16.
58. Usman, M.; Abdelmoula, M.; Hanna, K.; Grégoire, B.; Faure, P.; Ruby, C., FeII induced mineralogical transformations of ferric oxyhydroxides into magnetite of variable stoichiometry and morphology. *Journal of Solid State Chemistry* **2012,** *194*, 328-335.
59. Peacock, C. L.; Sherman, D. M., Copper(II) sorption onto goethite, hematite and lepidocrocite: a surface complexation model based on ab initio molecular geometries and EXAFS spectroscopy1 1Associate editor: D. L. Sparks. *Geochimica et Cosmochimica Acta* **2004,** *68*, (12), 2623-2637.
60. Weng, L. P.; Van Riemsdijk, W. H.; Hiemstra, T., Cu2+ and Ca2+ adsorption to goethite in the presence of fulvic acids. *Geochimica Et Cosmochimica Acta* **2008,** *72*, (24), 5857-5870.
61. Turel, I., The interactions of metal ions with quinolone antibacterial agents. *Coordination Chemistry Reviews* **2002,** *232*, (1), 27-47.
62. Chen, Z.; Xiong, R. G.; Zuo, J.; Guo, Z.; You, X.-z.; Fun, H.-K., X-Ray crystal structures of Mg2+ and Ca2+ dimers of the antibacterial drug norfloxacin. *Journal of The Chemical Society-dalton Transactions* **2000**, 4013-4014.
63. Yan, Y. P.; Wan, B.; Mansor, M.; Wang, X. M.; Zhang, Q.; Kappler, A.; Feng, X. H., Co-sorption of metal ions and inorganic anions/organic ligands on environmental minerals: A review. *Sci Total Environ* **2022,** 149918.
64. Xu, H.; Xu, D. C.; Wang, Y., Natural Indices for the Chemical Hardness/Softness of Metal Cations and Ligands. *Acs Omega* **2017,** *2*, (10), 7185-7193.
65. Audette, Y.; Smith, D. S.; Parsons, C. T.; Chen, W.; Rezanezhad, F.; Van Cappellen, P., Phosphorus binding to soil organic matter via ternary complexes with calcium. *Chemosphere* **2020,** *260*, 127624.
66. Yan, Y.; Wan, B.; Zhang, Y.; Zhang, L.; Liu, F.; Feng, X., In situ ATR-FTIR spectroscopic study of the co-adsorption of myo-inositol hexakisphosphate and Zn(II) on goethite. *Soil Research* **2018,** *56*, (5), 526-534.
67. Lenhart, J. J.; Bargar, J. R.; Davis, J. A., Spectroscopic Evidence for Ternary Surface Complexes in the Lead(II)–Malonic Acid–Hematite System. *J Colloid Interf Sci* **2001,** *234*, (2), 448-452.
68. Wan, B.; Yan, Y. P.; Zhu, M. Q.; Wang, X. M.; Liu, F.; Tan, W. F.; Feng, X. H., Quantitative and spectroscopic investigations of the co-sorption of myo-inositol hexakisphosphate and cadmium(II) on to haematite. *European Journal of Soil Science* **2017,** *68*, (3), 374-383.
69. Flynn, E. D.; Catalano, J. G., Competitive and Cooperative Effects during Nickel Adsorption to Iron Oxides in the Presence of Oxalate. *Environ. Sci. Technol.* **2017,** *51*, (17), 9792-9799.